



HAL
open science

Combustion and pollutant emission characteristics of argan nut shell (ANS) biomass

Yassine Rahib, Toufik Boushaki, Brahim Sarh, Jamal Chaoufi

► To cite this version:

Yassine Rahib, Toufik Boushaki, Brahim Sarh, Jamal Chaoufi. Combustion and pollutant emission characteristics of argan nut shell (ANS) biomass. *Fuel Processing Technology*, 2021, 213, pp.106665. 10.1016/j.fuproc.2020.106665 . hal-03173858

HAL Id: hal-03173858

<https://hal.science/hal-03173858>

Submitted on 3 Feb 2023

HAL is a multi-disciplinary open access archive for the deposit and dissemination of scientific research documents, whether they are published or not. The documents may come from teaching and research institutions in France or abroad, or from public or private research centers.

L'archive ouverte pluridisciplinaire **HAL**, est destinée au dépôt et à la diffusion de documents scientifiques de niveau recherche, publiés ou non, émanant des établissements d'enseignement et de recherche français ou étrangers, des laboratoires publics ou privés.



Distributed under a Creative Commons Attribution - NonCommercial 4.0 International License

1 **Combustion and pollutant emission characteristics of argan nut** 2 **shell (ANS) biomass**

3 **Yassine Rahib^{1, 2, *}, Toufik Boushaki¹, Brahim Sarh¹, Jamal Chaoufi²**

4 *Corresponding author: yassine.rahib@cns-orleans.fr, yassine.rahib@gmail.com;

5 ¹ Institute of Combustion, Aerothermal, Reactivity and Environment (ICARE)-CNRS UPR3021,
6 45071 Orléans Cedex 2, France.

7 ² Laboratory of Electronics, Signal Processing and Modelling Physics, Department of Physics, Ibn Zohr
8 University, 80000 Agadir, Morocco
9

10 **Abstract**

11 This paper presents an experimental study of argan nut shell (ANS) combustion in a lab-scale
12 furnace. Biomass composition, properties and microstructures were determined. Combustion
13 behaviour, fuel burn rate (FBR), pollutants (CO and NO_x), modified combustion efficiency
14 (MCE) and ash analysis were investigated. A comparison with wood pellets (WP) complying
15 with the ENplus Standard was performed. The impacts of air flow rate and particle sizes on
16 the combustion characteristics were analysed and discussed using three average ANS particle
17 lengths: 5-8 mm, 10-18 mm and 25-30 mm. The results show that the smallest length of ANS
18 particles induced a higher FBR and a regular distribution of the flame shapes compared to the
19 other sizes and to wood pellets. Furthermore, the combustion temperatures, CO emission and
20 MCE values were improved with the highest air flow rate used. CO emission was strongly
21 affected by the operating conditions while NO_x was very low for all selected cases. [Elemental](#)
22 [ash composition reveals that no ash agglomeration was observed during experiments in terms](#)
23 [of alkali index. Moreover, the obtained ash was in the form of powder instead of](#)
24 [agglomerated particles. This experimental investigation improves the understanding of the](#)
25 [operational characteristics and the combustion effect of ANS biomass.](#)

26
27 **Keywords:** Biomass combustion, argan nut shell, combustion behaviour, fuel burn rate,
28 pollutant emissions, ash analysis.

29 **1. Introduction**

30 Nowadays, there is significant interest in biomass feedstock for applications in green
31 energy as these materials represent an abundant, clean and renewable alternative energy
32 resource. In fact, biomass is considered as the fourth largest source of energy following
33 petroleum, coal and natural gas, with a current world demand for energy estimated at 53 EJ
34 [1]. Most applications of this global energy supply concern an assortment of energy needs,
35 including generating electricity, heating homes, cooking purposes and some industrial
36 applications [2]. However, a major part of the rural population in developing countries is
37 dependent on biomass, mainly as traditional fuel for cooking and heating. Agricultural
38 residues are the most widely available biomass materials with a high energy potential.
39 Werther et al. [3] estimated that over three billion tons of agricultural residues are generated
40 world-wide. In addition, this resource is considered to be less controversial than fossil fuels,
41 low cost and thus represents an important energy resource for countries with a massive
42 agricultural production.

43 The present study concerns the energy recovery of agricultural waste in the Mediterranean
44 basin. Argan is one of the agricultural resources producing this waste during the argan oil
45 production process; most of the waste is generated by the argan nut shell (ANS) [4]. The ANS
46 can be considered as an attractive source of biomass, since it is procurable in abundance and
47 does not contend with food production. The raw materials of ANS used in this work were
48 from the region of Sousse-Massa-Draa (southwestern Morocco) in which the development is
49 based on agricultural activities. The annual production of ANS is estimated at 60 000 tons per
50 year.

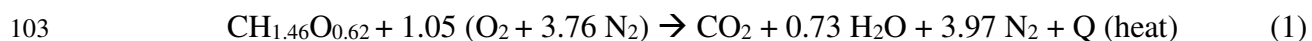
51 Among thermochemical conversion processes, combustion is a promising technology and
52 the most common option for biomass conversion [5]. Fixed-bed combustion is considered a
53 suitable and routine technique to optimize and transform agricultural residues into thermal

54 energy [6]. Studies on the combustion characteristics of fixed beds of biomass have been
55 reported by many papers. Khlifi et al. [7] studied the combustion of briquettes prepared from
56 olive mill solid wastes in the same reactor as the one used herein. They reported the influence
57 of the binder added to the prepared briquettes on combustion efficiency and pollutant
58 emissions. Khor et al. [8] and Cepic et al. [9] investigated the combustion characteristics of
59 straw in a fixed-bed reactor. Roy et al. [10] reported the combustion and emission results
60 obtained during the burning of four biomass pellets in a prototype pellet furnace. Elmay et al.
61 [11] studied the energy recovery of date palm residues from Tunisia, in a domestic pellet
62 boiler. The combustion parameters such as air flow and fuel particle size have been
63 investigated in the literature. Ryu et al. [12] experimentally investigated the effect of particle
64 size and air flow on the combustion characteristics of four biomass samples by determining
65 equivalence ratio, combustion temperature, ignition and burning rate. Rahib et al. [13] briefly
66 presented the combustion and emission characteristics of raw argan nut shell (ANS) in a
67 fixed-bed reactor. The focus was placed on the relationship between the nourishing tissue of
68 the argan almond and SO₂ emissions. Onabanjo et al. [14] studied the combustion
69 performance of human faeces by determining the combustion temperature, the fuel burn rate
70 and the combustion efficiency. They varied air flows, biomass sizes, bed heights, and fuel
71 ignition mode parameters in order to determine the optimum conditions for converting the
72 faecal biomass into energy. Meng et al. [15] examined the effect of varying corn straw lengths
73 and primary air flow on the combustion characteristics. They suggested that these two
74 parameters directly affect the burning rate, the bed temperature, the combustion emissions and
75 the boiler efficiency. The focus of our experimental research was to identify the conditions
76 that can lead to improved combustion of ANS in biomass combustion installations with ~50
77 MW output.

78 To comprehend the combustion process of ANS, the present paper investigates the
79 influence of particle lengths and air flows on combustion quality in a laboratory furnace. To
80 the best of our knowledge, no studies have been reported to date in the literature on the
81 combustion performance of ANS in a laboratory combustor. The first part of this work is a
82 parametric study to analyse the effect of different air flows. Measurements were carried out
83 on raw ANS and three different particle lengths chosen to analyse the size effect on
84 combustion. A comparison with wood pellets was performed. Results include flame structures
85 and stabilities for all the selected samples as well as ash analysis at different running
86 conditions. In view of the absence of ANS combustion studies, this work would be of great
87 interest to biomass combustion studies.

88 **2. Materials and methods**

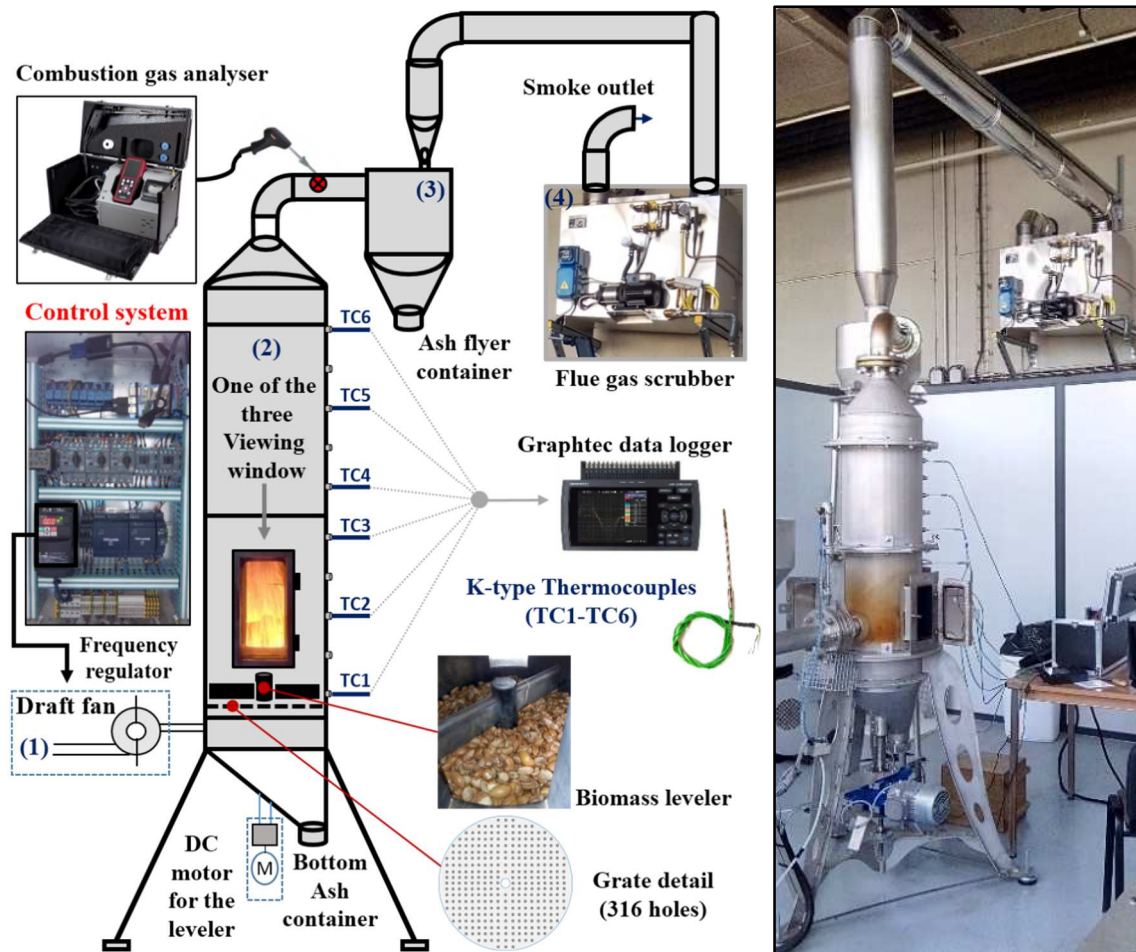
89 This study uses the ANS as raw biomass for combustion. Physicochemical characterization
90 was checked through ultimate and proximate analyses as well as the energy content
91 measurement. Ultimate analysis was carried out, using a FLASH 2000 CHNS/O analyser
92 (Thermo Scientific), to determine carbon (C), hydrogen (H), oxygen (O), nitrogen (N) and
93 sulphur (S) weight fractions. Proximate analysis was done using a Shimadzu analyser DTG-
94 60 according to the ASTM standard procedures. A more detailed description of the
95 experimental protocol can be found in our previous work [16]. A calorimetric bomb (Parr
96 2100) was used to measure the high heating value (HHV). The low heating value (LHV) was
97 calculated based on water and ash free contents. The energy density was obtained by
98 multiplying bulk density by the LHV. The empirical formula was computed based on C, H
99 and O content (masse fractions from ultimate analysis). By taking Carbone as reference, the
100 empirical formula of ANS is calculated as $\text{CH}_{1.46}\text{O}_{0.62}$ (where 1.46 and 0.62 represent H/C and
101 O/C molar ratios). The basic chemical reaction of ANS stoichiometric combustion can be
102 written as:



104 This equation was used to determine the theoretical air-fuel ratio.

105 A scanning electron microscope (SEM) was used to determine the physical nature of raw
106 ANS and ash at different magnifications. The equipment used was a JEOL JSM-IT100 SEM
107 model, connected to a dispersive energy X-ray spectroscopy (EDS) unit which was used to
108 access elemental composition in a semi-quantitative way. To set up this experiment, the tested
109 material was stuck on a thin layer of carbon.

110 Combustion of the ANS took place in a batch fixed-bed reactor. This device was
111 developed at ICARE-CNRS to investigate the thermochemical conversion process of
112 agricultural biomasses. Fig. 1 shows a schematic diagram of the experimental setup which
113 consists of: (1) an air fan adjusted by a frequency regulator (0-50 Hz), (2) a combustion
114 chamber composed of: a bottom ash recovery, a fixed grate, a rotating leveller, then a
115 confinement where the flame arises, (3) a cyclone connected by a flue pipe from the
116 combustion chamber outlet, (4) a flue gas scrubber.



117
118 **Fig. 1.** Experimental combustion setup.

119 The main components and measuring devices of the experimental rig are also illustrated.
120 The combustion chamber is divided into two compartments. It can be equipped with ten K-
121 type thermocouples inserted into the chamber centre to monitor the variation in flame and
122 maximum temperatures. Table 1 summarizes specific positions of the used thermocouples
123 (TC1-TC6). The temperature profiles were recorded every second by a Graphtec data logger.

124 **Table 1** Positions of the thermocouples along the combustion chamber.

Number	Distance from the grate (mm)
TC 1	55
TC 2	195
TC 3	335
TC 4	455
TC 5	595
TC 6	735

125 In the experiments, the composition and temperatures of the combustion gases were
126 measured in-situ at the combustion chamber outlet. Before analysing the flue gas, the
127 apparatus was calibrated. All emission profiles were recorded in the steady state zone. The
128 gas analyser used (Kimo KIGAZ 500) incorporates infrared and electrochemical measurement
129 techniques. The maximum response time of this instrument is less than 50 s. Therefore, a
130 sampling duration of 1 min was used to obtain stable values. At the beginning of each
131 experimental test, 1 kg of ANS is placed on the grate. Then, the leveller is switched on to
132 establish homogeneous distribution of the biomass bed. Afterwards, ignition of the biomass is
133 started on the entire surface of the bed using a gas blow torch and a small amount of liquid
134 fuel to promote the onset of combustion. A long-distributed flame throughout the upper
135 surface of the bed indicates a successful ignition and combustion test (see Fig. 2). The air
136 enters from the boiler bottom through the bed into the combustion chamber. The experimental
137 protocol followed is relevant for fixed grate and domestic boilers since (a) this configuration
138 can present the same contact between biomass particles in the bed, (b) the biomass
139 successively undergoes drying, devolatilization and char combustion and (c) geometric and
140 operational configurations relating to the aspect ratios of biomass particles, dimensions of the
141 bed and the flow paths of combustion gases are the same. Thus, some of the investigations
142 made herein could be quantitatively applicable to industrial combustion systems.

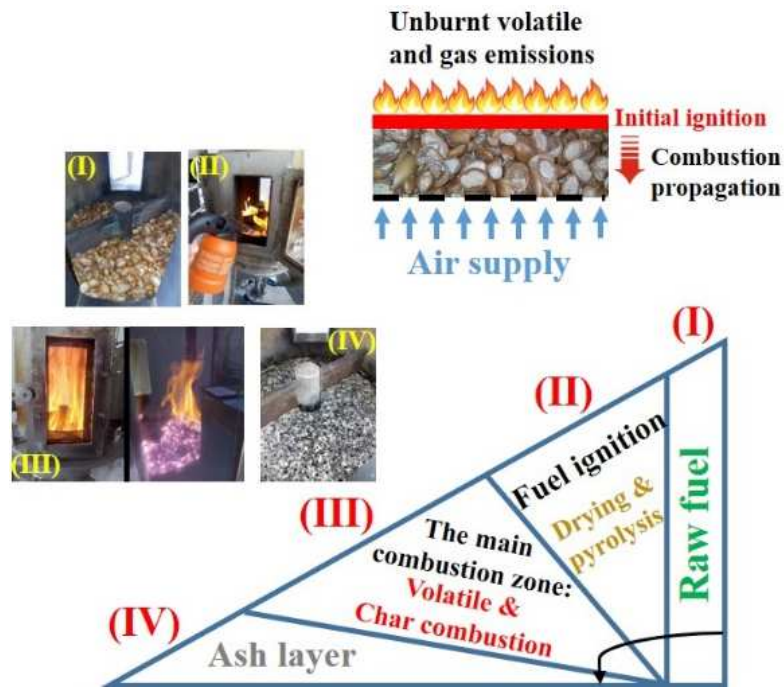


Fig. 2. Experimental procedure of the combustion tests.

The flows used in this study were 36, 72, 108, 144 and 180 m³.h⁻¹ corresponding to 528, 1057, 1585, 2113 and 2642 kg.m⁻².h⁻¹, respectively (in mass flow). At the end of each combustion test, the remaining ashes (bottom and fly ash) were collected and weighed. The optimum operating conditions for the ANS combustion were determined by varying air flow and particle lengths. The key performance of the process was assessed quantitatively by determining: the modified combustion efficiency (MCE), the fuel burning rate (FBR), the combustion temperatures, the average concentration of the combustion gases and the flame structures.

The MCE under different operating conditions was calculated based on CO and CO₂ emissions as described in equation (2):

$$\text{MCE (\%)} = \text{CO}_2 (\%) / [\text{CO}_2 (\%) + \text{CO} (\%)] \quad (2)$$

The FBR (g s⁻¹) as expressed in equation (3) signifies the time required for complete combustion of the biomass fuel consumed, at the end of each individual experiment, in mixture with air. It indicates the rate of energy released into the system.

159
$$\text{FBR (g s}^{-1}\text{)} = m_f(\text{g}) / t(\text{s}) \quad (3)$$

160 The FBR can be used to evaluate the biomass bed velocity (BBV) which was calculated by
 161 equation (4). Generally, the BBV increases with increase of FBR.

162
$$\text{BBV (mm.s}^{-1}\text{)} = \text{FBR (kg.s}^{-1}\text{)} / [\text{Bulk density (kg.m}^{-3}\text{)} * \text{grate area (m}^2\text{)}] \quad (4)$$

163 The end of each combustion experiment was selected to be the time moment when the
 164 temperature recorded from TC1 or TC2 decreased below 250 °C. At each air supply and fuel
 165 particle length, the performance criteria were tested in the steady state zone (flaming mode)
 166 when there was almost no change in flame temperature.

167 In order to shed light on the evolution of the combustion gas concentrations and
 168 temperature, we studied the impact of excess air on the combustion of ANS. The excess air is
 169 determined indirectly by measuring the concentration of unreacted oxygen in the flue gaz. A
 170 better approximation of the excess air can be computed using equation 5 [17].

171
$$\% \text{ Excess Air} = \frac{O_2 - \%CO/2}{20.9 - (O_2 - \%CO/2)} * 100 \quad (5)$$

172 The concentrations of O₂ and CO are obtained from sampling the gas at the combustion
 173 chamber outlet. The air factor (λ) and the equivalence ratio (ϕ) are deduced by:

174
$$\lambda = \frac{\% \text{ Excess Air}}{100} + 1 ; \text{ equivalence ratio (ER)} = \phi = \frac{1}{\lambda} \quad (6)$$


175 **3. Results and discussion**

176 **3.1. Biomass characterization**

177 Energy content, ultimate and proximate analyses of the raw sample are summarized in
 178 Table 2. The relatively high moisture content of ANS (9.5%) is in the range of some biomass
 179 sources used in thermal conversions [18]. However, the low ash content will positively impact
 180 the combustion efficiency and eliminate slag formation in the boiler. The high content of
 181 volatiles (61%) is an attractive characteristic that can improve the ignition process during
 182 combustion. The carbon and hydrogen contents were found to be 51.3 and 6.32%

183 respectively. ANS is also listed to have an impressively high heating value (HHV = 18.3
 184 MJ.kg⁻¹) despite the significant oxygen content. A critical property of biomass materials is
 185 bulk and energetic density, which are linked to storage and transport costs [19]. The values
 186 found for these two properties were 596 Kg.m⁻³ and 10.13 GJ.m⁻³ (for bulk and energetic
 187 density, respectively). This indicates that ANS can be an excellent candidate for
 188 thermochemical conversion [16,19,20]. Moreover, the hardness of ANS makes their storage
 189 and transport easier and ensures their long durability. The low values of N and S are a good
 190 indicator concerning the release of NO_x and SO_x pollutants to the atmosphere [16]. The
 191 theoretical air volume per kg fuel, calculated based on the ultimate analysis of the fuel, was
 192 found to be 4.75 Nm³.kg⁻¹. It refers to the amount of air necessary to complete combustion.
 193 The stoichiometric air fuel ratio (AFR) was also calculated (6.23 kg-air/kg-fuel) to identify
 194 the amount of air and fuel required for complete combustion.

195 **Table 2** ANS biomass properties.

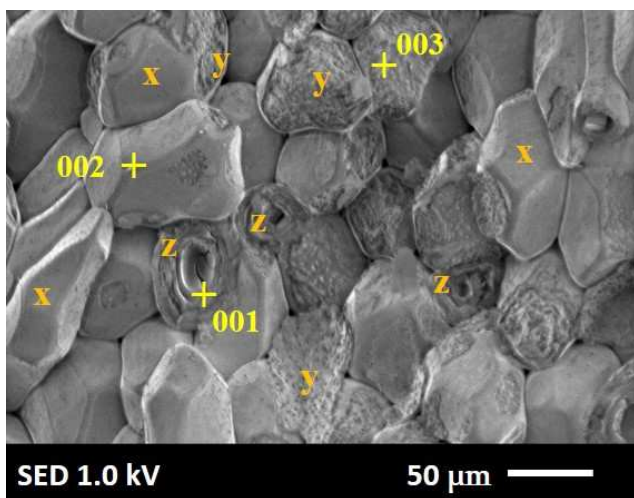
Photograph of the raw ANS particles 	Ultimate analysis ^a (%)				
	C	H	O	N	S
	51.33	6.32	42.345	0.005	n.d.
	Proximate analysis ^b (%) and bulk density (BD)				
	M	VM	FC	ash	BD
	9.5	61	28	1.5	596
Energy content ^b and stoichiometric calculation ^a					
LHV	ED	Equivalent formula	Stoichiometric air (Nm ³ .kg ⁻¹)	AFR	
17	10.13	CH _{1.46} O _{0.62}	4.75	6.22	

196 n.d.: not detected, M: moisture, VM: volatile matter, FC: fixed carbon, BD: bulk density (Kg.m⁻³), LHV: low heating value (MJ.kg⁻¹), ED:
 197 Energetic density (GJ.m⁻³), AFR: air fuel ratio (kg-air / kg-fuel).

198 ^a dry ash free basis, ^b as received basis

199 The photo in Fig. 3 shows the morphological characteristics of the raw sample. It was not
 200 subjected to any handling apart from natural dehydration in atmospheric air to eliminate
 201 external moisture. It can be seen that the ANS presents a polygonal organization composed of
 202 smooth and homogeneous zones indicated by the letters (x) and some roughness on its
 203 external surface (y). Damage to the external area of the material at the end of some particles
 204 (z) was observed, perhaps because of the fruit kernel crushing process. The SEM-EDS results

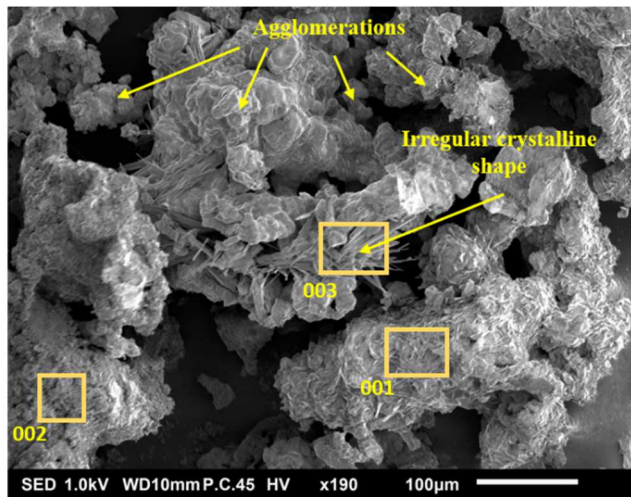
205 show that ANS is mainly composed of carbon (C) and oxygen (O). Minor amount of Al and
 206 Si were detected in the cracked zone (zone 001). Fig.3 includes the EDS analysis results.



	O	C	Al	Si
001	40.48	56.26	1.50	1.76
002	19.13	80.87		
003	33.98	66.02		
Average	31.20	67.72	1.50	1.76
Deviation	10.94	12.39	0.00	0.00

207 **Fig. 3.** Scanning electron microscope image and additional elemental analysis of the outer
 208 surface of ANS.

209 Fig. 4 shows the microstructure of the ash content of raw ANS. This material was obtained
 210 by the LOI (loss on ignition) method, i.e. raw ANS was combusted at 850 °C during three
 211 hours in a muffle oven according to the EN NF M03-003 procedure to eliminate all carbon
 212 content [21]. The morphology of the ash reveals the existence of small agglomerates (not
 213 significant) and the amorphous shape of particles (partially molten particles: spot 003). As we
 214 can see from elemental analysis, the ash contains mainly oxygen. The amount of carbon was
 215 very low and a significant amount of potassium K was identified (spot 1 and 2). Other major
 216 elements, in decreasing order, such as Mg, Na, P, Ca, S, Al and Si were detected.



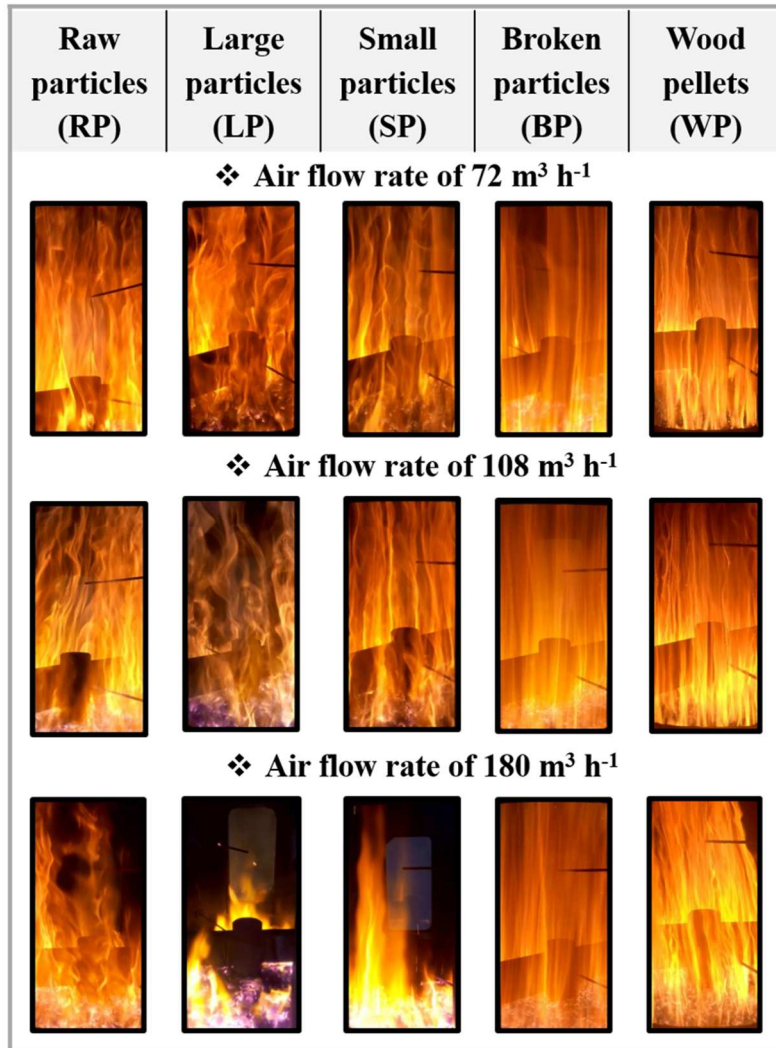
EDS	001	002	003	Av	S. Dv.
P	3.2	0.5	11.2	4.9	5.59
K	28.3	25.5	13.0	22.2	8.1
O	44.9	36.1	41.0	40.7	1.2
C	6.2	3.7	4.2	4.7	1.3
Na	6.4	0.9	19.8	9	9.7
Mg	1.4	27.6	3.4	10.82	14.6
Al	-	-	1.5	1.5	0
Si	1.6	1.12	0.6	1.1	0.5
S	0.37	-	3.3	1.8	2.1
Ca	7.67	4.47	1.8	4.6	2.9

Av: average, S. Dv.: standard deviation

217 **Fig. 4.** SEM-EDS analysis of ANS ash obtained by LOI method.

218 **3.2. Visual observation of the combustion**

219 A general trend of combustion behaviour in fixed beds was observed. Fig. 5 shows the
 220 flame images from the videos of ANS as a function of three air flows and the particle sizes.
 221 This flame represents the combustion of pyrolysis gas during the whole process [22]. The
 222 wood pellets (WP) were also included for the purpose of comparison. The higher air flow
 223 supply ($180 \text{ m}^3 \cdot \text{h}^{-1}$) affected combustion stability, slowed down the combustion process and
 224 extinguished the flame (cases LP (large particle) and SP (small particle)). In the RP (raw
 225 particle) case, it was noticed that a higher air flow did not extinguish the flame but limited its
 226 progress along the combustion chamber. This can be attributed to the presence of broken
 227 particles in the raw ANS, which need more oxygen to complete the burning process (see
 228 further explanations in section 3.4). In the BP (broken particle) and WP cases, the high air
 229 supply did not perturb the flame; the combustion seemed homogeneous, and the flame was
 230 very stable. With a lower air flow supply ($72 \text{ m}^3 \cdot \text{h}^{-1}$), the flame images in RP, LP, SP, BP and
 231 WP showed intense luminosity, which indicates the existence of some soot because of the rich
 232 regime of biomass. The luminosity decreased with increasing air flow, since oxygen addition
 233 improved the combustion process (fuel lean conditions).



234

235

236

Fig. 5. Images of visible flames from the combustion recording of ANS at different operating conditions and particle sizes. WP are added for comparison.

237

238

239

240

241

242

243

244

245

From a structure and stability point of view, flames in the case of BP under the studied air supply were characterized by a regular shape and a relatively smooth and continuous flame front. This can be explained by the existence of a pre-mixed zone in which the volatile gases released by the broken particles mixed well with the surrounding air. This behaviour is similar to premixed gas combustion as in [23] where the combustion reactions are mainly affected by chemical kinetics. The LP and SP probably take a lot of time to devolatilize [12,24], which contributes to delaying ignition and to a more irregular flame shape. The flame becomes increasingly stable when particle sizes decrease.

246 3.3. Effect of air flow

247 The combustion tests of raw ANS samples in varying air flow conditions were performed
248 to analyse the effect of this crucial parameter in achieving the highest combustion
249 performances. Fig. 6a-c reveals a typical flame temperature profile (a), combustion behaviour
250 (b) and combustion gas concentration (c) inside the reactor with a $36 \text{ m}^3 \cdot \text{h}^{-1}$ air supply (528
251 $\text{kg} \cdot \text{m}^{-2} \cdot \text{h}^{-1}$). The process can be divided into four stages as illustrated in Fig. 6a: (1) start-up
252 (2) steady-state (3) combustion of residual char and (4) switch off. Similar behaviour was
253 identified in the other air supply cases with some oscillation observed in the steady state zone.
254 Fig. 6b illustrates visual observations of the four stages of the combustion process. The steady
255 state zone was found to be characterized by homogenous (flame mode: blackening of bed
256 particles) and heterogeneous (flame was observed during char ignition) combustion
257 behaviour. The combustion of the char heats the bed without significant heat exchange to the
258 bordering flame. The first chute (stage 3) indicates the beginning of flame extinction. Once
259 the volatile flame extinguishes, the ANS bed starts to lose heat, whence the second slopes
260 (stage 4). Fig. 6c shows the gas emission profiles as a function of combustion time. The O_2
261 concentration decreased swiftly as the combustion process proceeded. This was followed by
262 an increase in CO_2 , CO , CH_4 and NO_x ($\text{NO} + \text{NO}_2$). The CO_2 content is predominant because
263 of the higher carbon content in ANS. When the biomass flame began to drop (Switch off: char
264 mode), the O_2 concentration began to rise, while CO , CO_2 , CH_4 , NO_x and SO_2 declined
265 regularly, indicating the end of combustion stage. Generally, the combustion process of ANS
266 was shown to be dominated by the flaming mode. The combustion of the remaining char, after
267 the extinction of the flame, was not a major event [20]. This behaviour was similar to that
268 reported in [25].

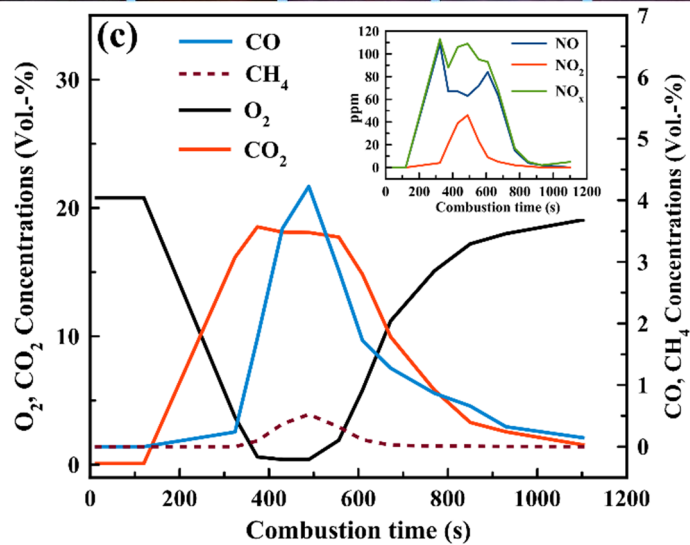
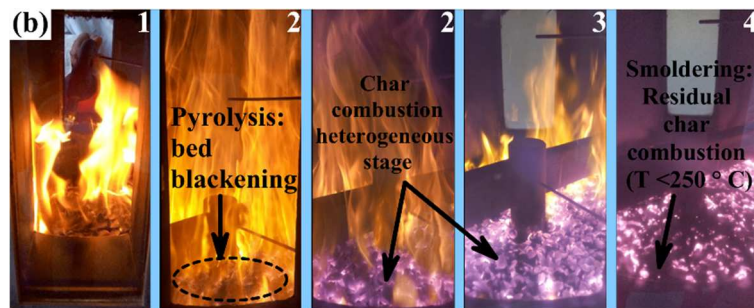
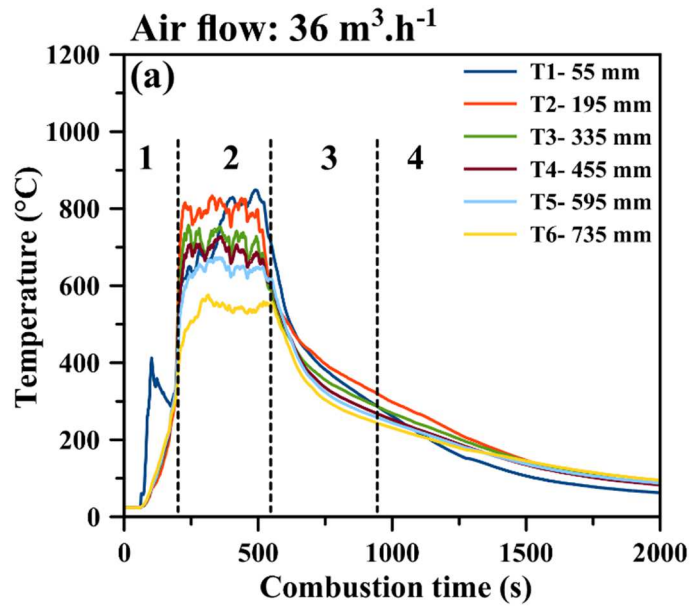
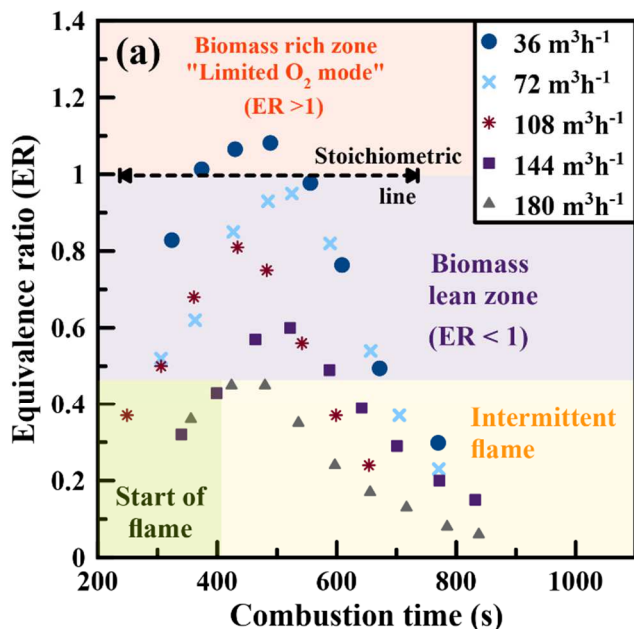


Fig. 6. Typical combustion results: (a) flame temperature (b) visual observation and (c) corresponding combustion gas concentrations (case of $36 \text{ m}^3 \cdot \text{h}^{-1}$ air supply).

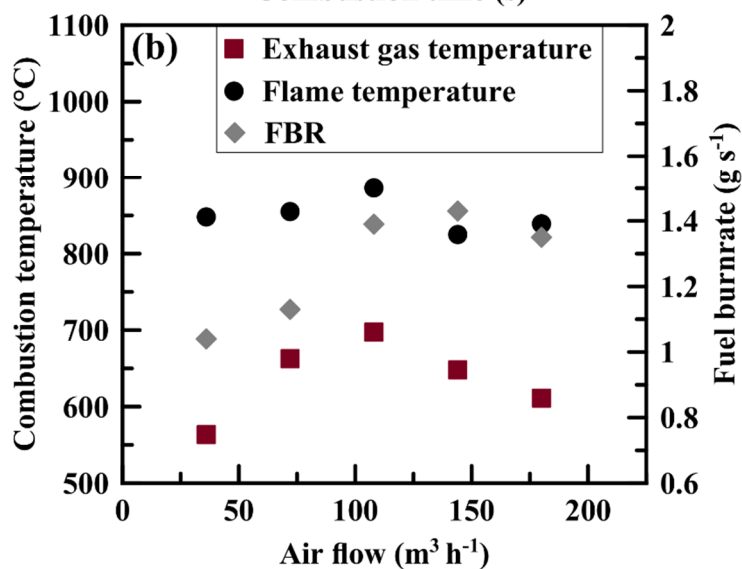
Fig. 7a-c illustrates the significant impact of air flow on the combustion process of raw ANS. Calculated equivalence ratios (ER) in the flame zone, (equations 5 and 6), are shown in Fig. 7a.

277 The bold arrow (dotted line) indicates the theoretical stoichiometric combustion regime. The
278 instantaneous ER measured at different air flow rates (except for $36 \text{ m}^3 \cdot \text{h}^{-1}$) is located in the
279 "sub-stoichiometric" fuel lean zone ($\text{ER} < 1$ at the interval of 300 and 700s) of the transient
280 combustion period. With an air flow supply of $36 \text{ m}^3 \cdot \text{h}^{-1}$, the rich regime appears ($\text{ER} > 1$) in
281 the combustion period between 370 and 550s. In this zone, all the oxygen was consumed
282 (temporary oxygen deficiencies: $\text{O}_2 < 0.1\%$) and high emissions of CO and CH_4 were
283 observed (see Fig. 6c). Moreover, the intermittent flame zone ($\text{ER} < 0.45$) characterizes the
284 rapid extinguishes of the flame due to convective cooling (when the air flows are not
285 favourable: Fig. 5, air flow rate of $108 \text{ m}^3 \cdot \text{h}^{-1}$). The results in Fig. 7b reveal that the maximum
286 flame temperature (registered by TC1 or TC2) increased progressively with increasing of the
287 air flow until a value of $886 \text{ }^\circ\text{C}$ corresponding to an air flow of $108 \text{ m}^3 \cdot \text{h}^{-1}$. Beyond this flow
288 rate, the flame temperature decreased with the increase of the air flow. The exhaust gas
289 temperature had the same behaviour, with a maximum value of $767 \text{ }^\circ\text{C}$ corresponding to the
290 same air flow. Similar behaviour was also observed in the case of FBR, which presented
291 maximum values of 1.39 and 1.43 g s^{-1} for an air flow of 108 and $144 \text{ m}^3 \cdot \text{h}^{-1}$, respectively.
292 The FBR decreased gradually with further increase in the air supply (case of $180 \text{ m}^3 \cdot \text{h}^{-1}$). Fig.
293 7c reveals that the modified combustion efficiency ranged from 88 to 97% as a function of the
294 studied range of the air flow (36 to $180 \text{ m}^3 \cdot \text{h}^{-1}$). It is shown that MCE increased then
295 decreased with the air flow, with a maximum value (97%) observed at $108 \text{ m}^3 \cdot \text{h}^{-1}$. The BBV
296 presented the same behaviour as FBR with maximum values at 108 and $144 \text{ m}^3 \cdot \text{h}^{-1}$
297 corresponding to the same air flows. As noted by Khor et al. [8], the combustion temperature
298 and burning rate of straw increased significantly with an increased in air flow velocity until a
299 critical point. Thereafter, they decreased with a further increase in primary air flow due to
300 convective cooling, because the impact of increased convection was stronger than the effect
301 of increased temperature at high flow rate. Onabanjo et al. [14] observed that the combustion

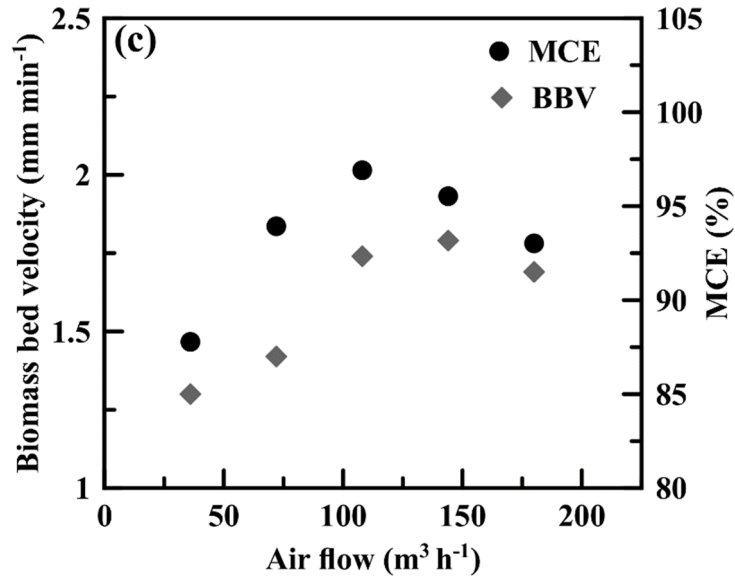
302 reaction of human faeces rapidly turned off when the air flow exceeded a critical value. They
 303 suggested that the excess air flow (unfavourable, i.e. convection by cooling) limits the flame
 304 propagation, reduces the combustion temperature and affects the combustion stability.



305



306



307 **Fig. 7.** Influence of the air flow on: (a) equivalence ratio (b) combustion temperature
 308 and FBR, (c) BBV and MCE.
 309

310 Fig. 8 shows the mean pollutant concentration calculated, converted and corrected at 10%

311 O₂ using the following formula, respectively [17] [26] :

$$C_{mean}(ppmv) = \frac{1}{\tau} \int_0^{\tau} [Concentration]_{Exp}(\tau) dt$$

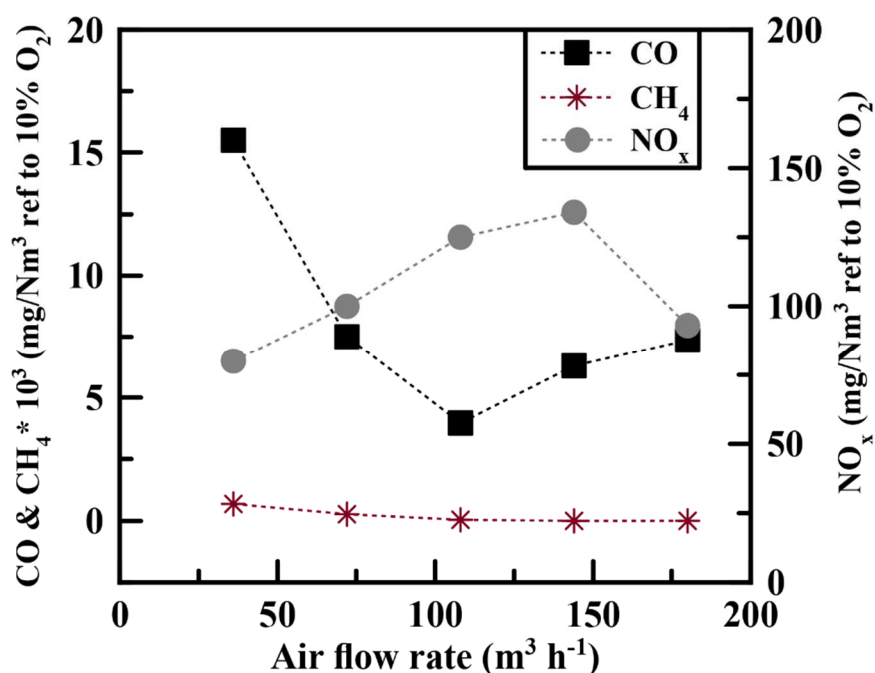
$$C_{mean}(mg.Nm^{-3}) = C_{mean}(ppmv) * \frac{\text{gram molecular weight}}{\text{molar volume}} \quad (7)$$

$$[Concentration]_{corrected \text{ at } X\% O_2} = [Concentration]_{Exp} * \frac{20.9 - X\%O_2}{20.9 - [\%O_2]_{Exp}}$$

312 where C_{mean} is the mean pollutant concentration; τ is the time of biomass combustion (s);
 313 molar volume at STP (0 °C and 1 atm.) = 22.414 l; $X\%O_2$ is the reference oxygen content in
 314 % volume and Exp is the measured concentration.

315 In this Figure, the effect of varying air flow on the combustion process is demonstrated.
 316 The CO concentration in the gas was very high ($1.5 \cdot 10^4 \text{ mg.Nm}^{-3}$) with an air flow of $36 \text{ m}^3.\text{h}^{-1}$
 317 ¹ because of the rich regime of biomass. It decreased progressively on increasing the air flow
 318 until a value of 3973 mg.Nm^{-3} corresponding to $108 \text{ m}^3.\text{h}^{-1}$. Afterwards, the CO concentration
 319 increased gradually at high air excess (144 and $180 \text{ m}^3.\text{h}^{-1}$) due to a high amount of unburnt

320 biomass, resulting in the increase in C char emissions (short residence time of ANS in the
 321 combustion zone). The NO_x emissions (calculated based on the measured concentrations of
 322 NO and NO_2) were relatively weak (below 140 mg.Nm^{-3} referred to 10% O_2 in the fume (Fig.
 323 8)). This was an expected positive result given the very low nitrogen content (0.005% on dry
 324 ash free basis). Emissions of CH_4 decreased from 688 mg.Nm^{-3} at $36 \text{ m}^3.\text{h}^{-1}$ to 3 mg.Nm^{-3} at
 325 $180 \text{ m}^3.\text{h}^{-1}$. With a $108 \text{ m}^3.\text{h}^{-1}$ air supply, the CH_4 value was found to be very low (44 mg.Nm^{-3}
 326 3).



327 **Fig. 8.** Mean emission concentration during combustion corrected at 10% O_2 .
 328

329 It is concluded in this first part that the optimal air supply for the fixed-bed combustion of
 330 1 kg of raw ANS was around $108 \text{ m}^3.\text{h}^{-1}$, which provided the highest flame and exhaust gas
 331 temperatures (886 and $698 \text{ }^\circ\text{C}$, respectively), the highest FBR and BBV (1.39 g s^{-1} and 1.35
 332 $\text{mm}^2 \text{ s}^{-1}$, respectively), the highest MCE (97 %) and lower concentrations of pollutant
 333 (especially CO). In this case, the ash mass was the lowest (<1%) among the other air flows
 334 applied, indicating that practically all the biomass was burned.





335

336

337 **3.4. Effect of particle size**

338 The ANS biomass was classified into three different ranges of lengths: large (2.5-3 cm),
 339 small (1-1.5 cm) and broken (< 8 mm). Table 3 displays photographs and the calculated bulk
 340 densities (BD) of each classified sample.

341 **Table 3** Classification of the three sizes from the raw ANS samples. Wood pellets are added
 342 for comparison purposes.

Samples	Large particles (LP)	Small particles (SP)	Broken particles (BP)	Wood pellets (WP)
photograph				
Length	2.5 – 3 cm	1 – 1.8 cm	< 8 mm	3.15 – 4 cm
BD*	556	592	642	650
Bed porosity	0.48	0.44	0.39	0.47

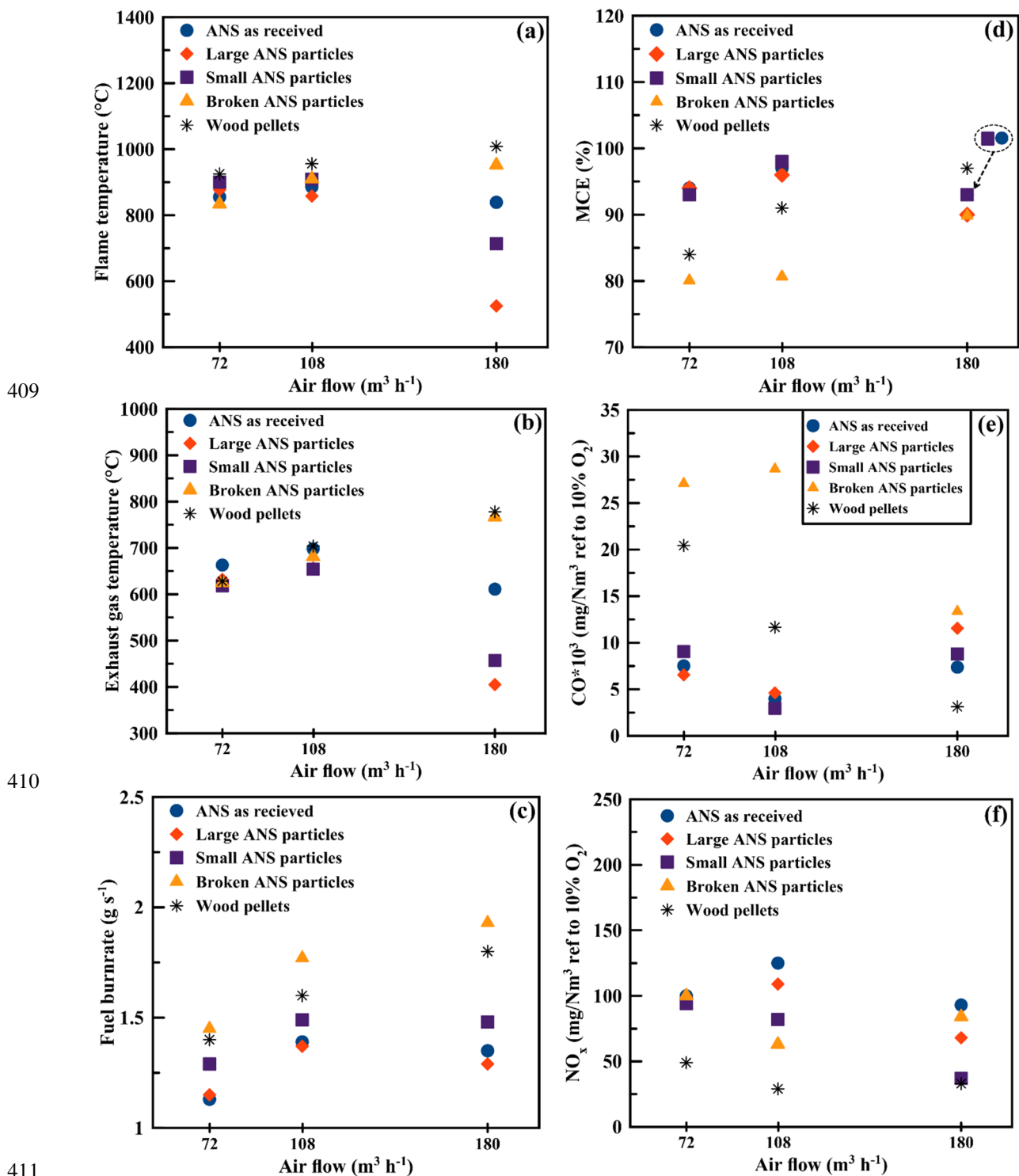
343 * BD: bulk density (kg.m⁻³). Measurement was done in quadruplicate, and the mean value is reported.

344 Fig. 9a-f presents the effect of varying ANS length on combustion temperatures, FBR,
 345 MCE, and CO and NO_x emissions (corrected at 10% O₂). For each case, the performances
 346 were assessed at three constant air flows of 72, 108 and 180 m³.h⁻¹, corresponding to weak,
 347 appropriate and excess air conditions, respectively (based on the results of raw ANS
 348 combustion). This can offer the possibility to investigate the effect of air flows and particle
 349 sizes at the same time. The results of raw ANS particles (RP) are included and a comparison
 350 with wood pellets is also reported. Fig. 9a and b show the influence of varying biomass length
 351 on the combustion temperature. For a low air supply (72 m³.h⁻¹), the small particles (SP)
 352 generated the maximum flame temperature while the broken particles (BP) gave the minimum
 353 flame temperature. The results show that flame temperature increased from 834 to 900 °C
 354 when the broken particles (BP) were replaced by SP. The two other cases (LP and raw

355 particles) fell between the BP and SP. For the appropriate air supply ($108 \text{ m}^3 \cdot \text{h}^{-1}$), the BP and
356 SP induced the same flame temperature, ($910 \text{ }^\circ\text{C}$), whereas the LP induced the minimum
357 flame temperature ($858 \text{ }^\circ\text{C}$) due to the short residence time in the combustion zone. Under
358 high excess air ($180 \text{ m}^3 \cdot \text{h}^{-1}$), the difference in flame temperature was very high for the three
359 ANS sizes. For example, the flame temperature was $525 \text{ }^\circ\text{C}$ for LP and $952 \text{ }^\circ\text{C}$ for BP. Results
360 concerning the exhaust gas temperature (see Fig. 9b) exhibited the same evolution as that of
361 flame temperature. The exhaust gas temperatures of BP and WP were very close. Fig. 9c
362 shows that the FBR evolution with the air flow was similar for LP and SP. Depending on the
363 air supply, BP had the highest fuel burn rate compared to the other particle sizes and WP. The
364 LP and raw particle (RP) cases yielded the lowest FBR. In the case of the lower air flow, FBR
365 was 1.13, 1.15, 1.29, 1.45 and 1.40 g s^{-1} for RP, LP, SP, BP and WP respectively. These
366 values increased under moderate air flow ($108 \text{ m}^3 \cdot \text{h}^{-1}$) to reach 1.39, 1.37, 1.49, 1.77 and 1.60
367 g s^{-1} for RP, LP, SP, BP and WP, respectively. Under a high air supply, the FBR decreased for
368 RP, LP and SP (1.35, 1.29 and 1.48 g/s , respectively) but continued to increase for BP and
369 WP (1.93 and 1.80 g s^{-1} , respectively). Fig. 9d presents the particle length effect on the
370 combustion efficiency. The MCE results of the different cases of ANS particle sizes are
371 completely different to the FBR results. The MCE value in the case of a $72 \text{ m}^3 \cdot \text{h}^{-1}$ air supply
372 was 94, 93, 80 and 84% for RP + LP, SP, BP and WP respectively. These values were found
373 to rise for all samples in the moderate air flow ($108 \text{ m}^3 \cdot \text{h}^{-1}$) to reach 97, 96, 98, 81 and 91%
374 for RP, LP, SP, BP and WP, respectively. For the highest air supply ($180 \text{ m}^3 \cdot \text{h}^{-1}$), MCE
375 declined for RP, LP and SP (93, 90 and 93%, respectively) but increased for the BP and WP
376 (90 and 97%, respectively). In the literature, some authors have studied the effect of biomass
377 size on combustion. El-Sayed et al. [24], found that the larger the size of the fuel particles, the
378 greater the probable residence time of the volatile gases within these particles. Ryu et al. [12]
379 proved that large particles (thermally thick) have a slow devolatilization rate and more

380 distributed heat transfer to the nearby particles. They noted that temperature gradients in the
381 biomass bed during combustion decrease with increasing particle sizes. This led them to
382 conclude that heat penetration to the cold particles below the hot ones is more extreme for
383 smaller particles. Luo et al. [27] demonstrated that the biomass fuel burn rate and maximum
384 combustion temperature increased with the decrease in particle size. The large particles
385 present a greater resistance to heat transfer, and therefore their internal temperature was
386 lower. In the present investigation, the optimal air supply for burning LP and SP was found to
387 be similar to that needed for raw ANS particles ($108 \text{ m}^3 \cdot \text{h}^{-1}$). Flame durations of 1kg ANS
388 combustion were 681, 579 and 726s for 72, 108 and $180 \text{ m}^3 \cdot \text{h}^{-1}$, respectively in case of the LP.
389 In the case of SP, the flame durations were 549, 558 and 628 for 72, 108 and $180 \text{ m}^3 \cdot \text{h}^{-1}$,
390 respectively. These results agree with those of El-Sayed et al. [24]. RP, LP and SP showed the
391 same behaviour for the three air flows used. They increased their performance when the air
392 flow was changed from low ($72 \text{ m}^3 \cdot \text{h}^{-1}$) to moderate ($108 \text{ m}^3 \cdot \text{h}^{-1}$) conditions, but decreased
393 regularly in higher air excess ($180 \text{ m}^3 \cdot \text{h}^{-1}$). For the RP, LP and SP, $180 \text{ m}^3 \cdot \text{h}^{-1}$ is an excessive
394 air flow during combustion, since it contributes to convective cooling of the biomass bed,
395 slows down the process and extinguishes the flame (see Fig. 3). Contrariwise, the
396 performance of BP and WP revealed an increasing trend when the air flow was increased. The
397 FBR and the maximum combustion temperature of BP were the highest for the high air flows
398 (108 and $180 \text{ m}^3 \cdot \text{h}^{-1}$) compared to the other sizes. This can be explained by the fact that when
399 raw particles (RP) of ANS were broken, their contact area with air was greater, which leads to
400 higher combustion reaction rates and greater air flow supply needs. The MCE value obtained
401 for air flow rates of 72 and $108 \text{ m}^3 \cdot \text{h}^{-1}$ was low (the case of BP), indicative of a poor mixing
402 process (high CO emissions) as indicated in Fig. 9e. However, an air flow of $180 \text{ m}^3 \cdot \text{h}^{-1}$
403 revealed a lower CO emission and a tolerable MCE value. Hence, it could be concluded that
404 broken particles can be burned better than large particles and reach better combustion

405 performances if the required compromise of mixing air and biomass is achieved. The yields of
 406 NO_x emissions were found to be below $140 \text{ mg}\cdot\text{Nm}^{-3}$ for all the experimented conditions (see
 407 Fig. 9f). This was expected since fuel-N, considered as the major source of NO_x [28], was
 408 very low.



412 **Fig. 9.** Effect of particle size on combustion temperature (a and b), FBR (c), MCE (d), CO
413 and NO_x emission (e and f, respectively).

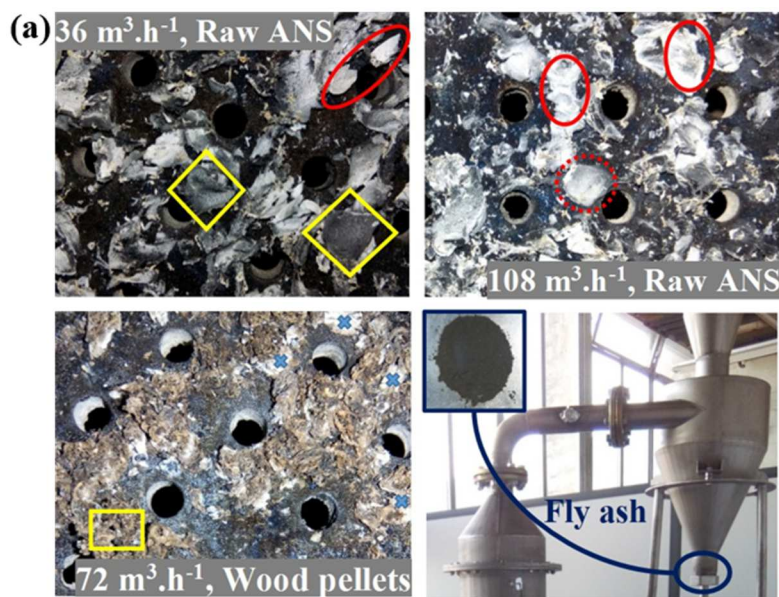
414

415

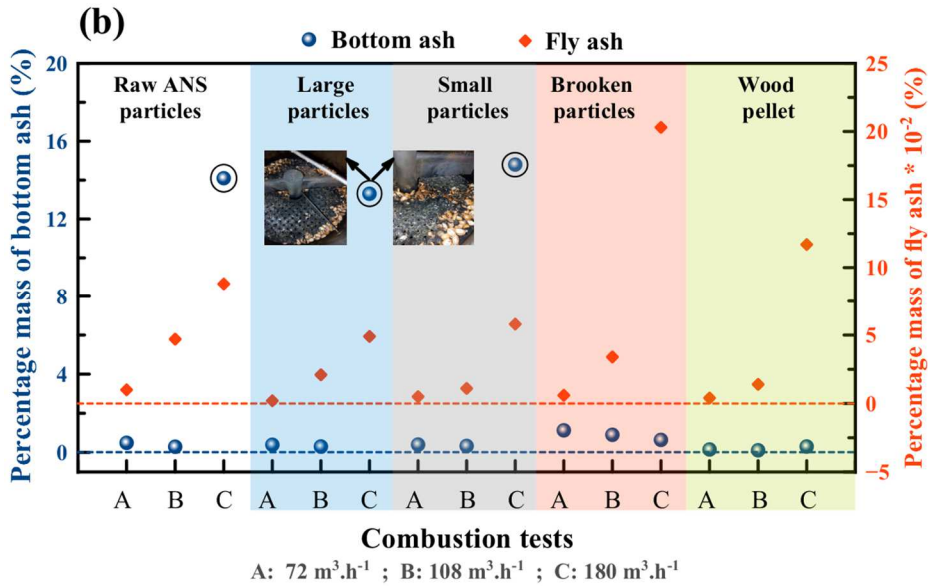
416 **3.5. Ash characterization**

417 The ash of fixed beds of ANS is defined as the amount of solid residue that remains at the
418 end of the combustion test. It is considered as a complex inorganic-organic mixture with a
419 heterogeneous and variable composition [29]. Knowledge of the physicochemical properties
420 of biomass ash is useful information in predicting the tendency to form deposits in boiler
421 components. In this study, the ANS and WP ash produced during laboratory scale combustion
422 included bottom and fly ash as shown in Fig. 10. In all the experiments, bottom ash
423 represented the major part of total ash. Coarse particles of unburned char end up as bottom
424 ash while finer ones flow out with gases in the form of fly ash. The colour of bottom ash
425 ranged from light grey and brown to black. At first glance, one can see that the ash particles
426 of raw ANS can be classified into three parts: unburned char marked by yellow diamonds
427 (darker coloured biomass ash), incomplete char combustion marked by the red dotted circle,
428 and totally combusted particles corresponding to the clearest particles (inorganic matter,
429 particularly alkali and alkaline earth metals) marked by red circles in the corresponding
430 figures. A high amount of unburned char was identified in the case of a low air supply (36
431 m³.h⁻¹), indicating poor combustion efficiency. On the other hand, it can be seen that the
432 residual bottom ash of WP was composed of solid parts (unburned biomass) which have the
433 same colour as the raw sample (yellow square). The completely burned parts of WP are
434 marked by a blue cross. The high unburned WP can be explained by the high biomass regime
435 with an air supply of 72 m³.h⁻¹. No clear sign of sintering and agglomeration was observed
436 from the ANS ash displayed in Fig. 10a. Fly ash collected from the cyclone container was
437 characterized by a black colour, i.e. a high-unburnt carbon content. Fig. 10b shows the

438 percentage mass ($= \frac{\text{masse of ash}}{\text{initial mass of biomass bed}} * 100$) of bottom and fly ash of ANS during
 439 combustion tests. It is observed that the bottom ash is generally low (<2%) except for raw,
 440 large and small particles under excess air conditions (C). This can be explained from the
 441 above results, which reveal that these kinds of particles have shown unstable combustion
 442 behaviour with limitations in flame mode. Therefore, the bottom ash is mainly generated by
 443 the quantity of unburnt particles as shown in the photos included in Fig.10b. The amounts of
 444 fly ash show an increasing trend with increasing air flow rate. The maximum fly ash content
 445 is observed for the broken particles at $180 \text{ m}^3 \cdot \text{h}^{-1}$. These particles with high air flow rate show
 446 stable combustion and well distributed flame throughout the bed. After the flame was
 447 extinguished, the oxidation of the char part, consisting of small particles, was very short,
 448 which favoured the transport of ash particles by the fumes. For a low air flow rate (A), fly ash
 449 is not detected.



450



451
452 **Fig. 10.** Photographs of the ANS and WP combustion ashes in the grate (a) and the
453 distribution of ash percentage mass during combustion tests (b).

454 SEM/EDS was used to analyse the residual ash of the studied samples by combining a
455 visual image with elemental analysis. Fig. 11a-c illustrates the morphology of bottom ash
456 from raw ANS and wood pellet samples at different operating conditions. Figures X, Y and Z
457 show the zones marked in Fig. 11c at higher magnifications. The ash of BP of ANS was found
458 to be mainly composed of unshaped particles and fine materials (Fig. 11a). These abundant
459 unshaped particles showed a porous microstructure (Fig. 11b). Wood pellet ash showed mixed
460 morphologies with particles of different shapes and sizes. In the X, Y and Z areas, the
461 dominant number of unshaped materials in WP can be clearly seen (Fig. 11c). Fig. 11a-c also
462 shows the selected areas indicated by crosses and rectangles (from 001 to 010) where the semi
463 quantitative elemental analysis (atom %) was performed. The results of the ash analysis are
464 summarized in Table 4. The morphology of ANS ash obtained during fixed-bed combustion
465 was different from that obtained by LOI (see Fig. 4). No visible aggregation or crystal
466 particles were observed. The porous structure (spots 1 and 4) was mainly composed of carbon
467 (76 %), oxygen (18%) and potassium (5%). Other elements were found in minor amounts
468 (Na, Mg and Ca). The Cl and Al percentage in the bottom ash samples was negligible. WP
469 ash (see Fig. 11c) also contained significant quantities of carbon and oxygen. Ca, K, P and

470 Mg were detected as major elements (>1%), and Na, Si and Al as minor elements (<1%). S
471 and Cl elements were not detected. The alkaline index (AI) is the amount of alkaline oxide in
472 the biomass per unit of energy (kg alkaline per GJ). It was used in this study as an indicator of
473 fouling and slag formation. The existence of such problems is likely for an AI greater than
474 0.17 kg.GJ⁻¹ and certain for a value greater than 0.34 kg.GJ⁻¹ [8,12,30]. Fixed-bed combustion
475 of ANS gave an alkaline index of 0.17 kg.GJ⁻¹ and did not contribute to agglomeration. For
476 WP a low AI value was obtained (0.05 kg.GJ⁻¹). In other terms, proximate analysis of ANS
477 reveals a very low ash content (<1.5 %). During combustion, the obtained smaller particle
478 size of ash (with no agglomeration) can be justified by the low temperature operation of the
479 boiler (<1000°C). Additionally, the obtained low values of Na and Cl (minor elements:
480 generally, <1%) in ANS ash are a good indicator for limiting the tendency of producing
481 agglomerates. This can be justified with the fact that higher percentages of chloride (NaCl)
482 contribute in a low ash-melting temperature, as reported in [31].

483 Fig. 11d-f shows the morphology of ANS and WP fly ash. Local chemical composition
484 (spot I-XI) was carried out by EDS and the results are also summarized in Table 4. The ANS
485 fly ash examined (Fig. 11d and e) mainly contained particles of various shapes and sizes. In
486 general, prismatic, polyhedral, spherical and fibrous particles were observed. Coarse particles
487 (spots II and III) with high specific surfaces represented typical organic materials. On the
488 contrary, the fine particles were roughly spherical (dotted red circles) and mainly contained O,
489 K, Si and Ca, while the amount of unburned carbon was minimal. Elemental concentrations of
490 P, Na, Mg, Al and S were considerably lower than those of other elements. WP Fly ash (see
491 Fig. 11f) mostly contained coarse and other fibrous particles resembling the original structure
492 of wood fibre. The dark and fibrous particles were mainly formed of carbon and oxygen and
493 came mainly from the unburnt char. In addition, the clearest and brightest particles were
494 composed of inorganic materials, in particular alkali (K) and alkaline earth (Ca), as well as S

495 and Cl (as minor elements: 0.1-1%). The large amount of unburnt carbon in ANS and WP fly
496 ash is mainly due to incomplete combustion of the char part. After flame extinction, the
497 primary air cools the combustion chamber and transports the fine particles of char to the
498 cyclone. Finally, under the moderate air flow ($108 \text{ m}^3 \cdot \text{h}^{-1}$), the bottom and fly ash content of
499 ANS were negligible (<0.5 and $<0.05\%$, respectively), i.e. losses due to unburnt carbon can
500 be neglected.

501

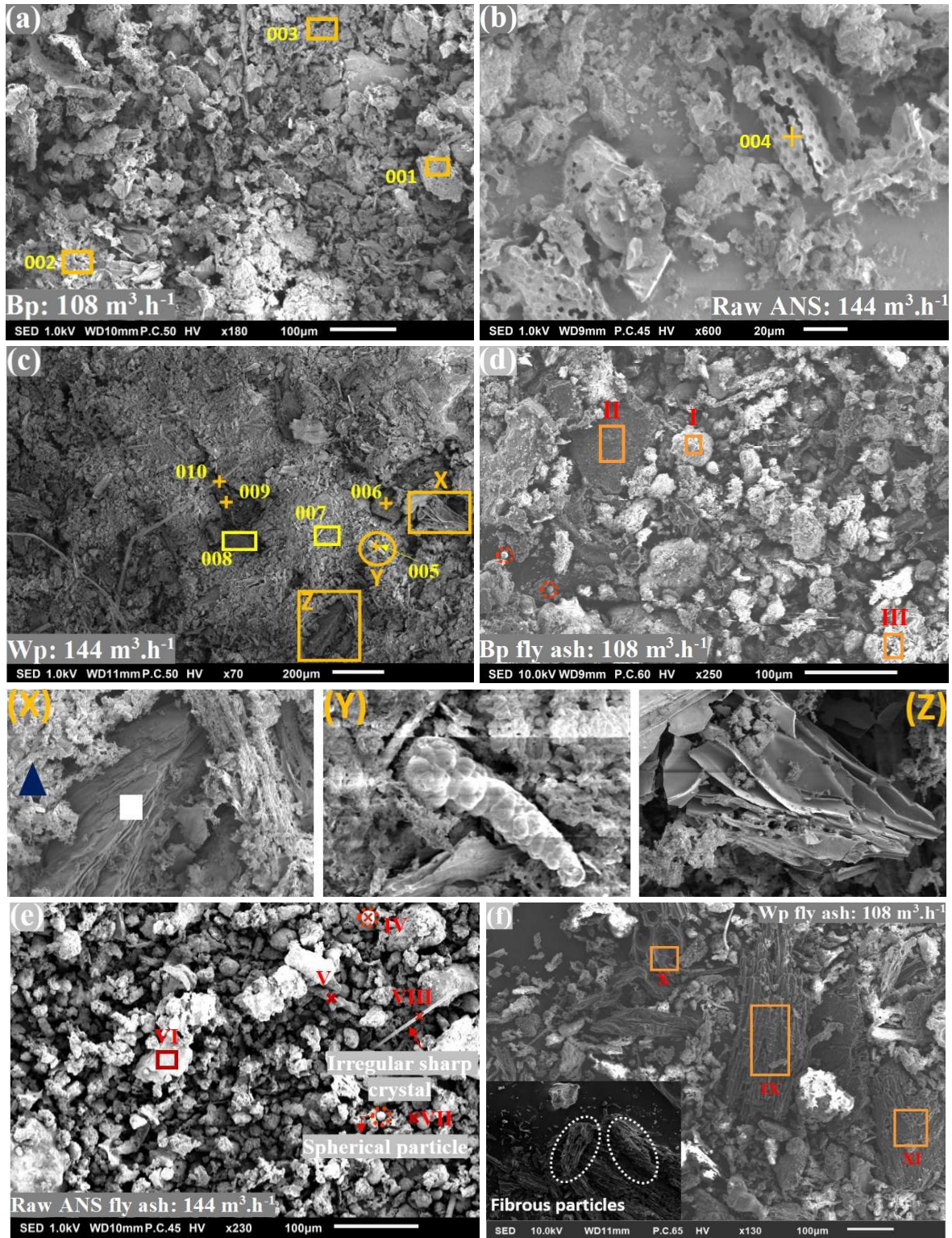


Fig. 11. SEM images of ANS and WP ash at different operating conditions: bottom ash (a-c) and fly ash (d-f).

509 **Table 4** EDS analysis (atom %) of ANS and WP ash.

EDS	P	K	O	C	Na	Mg	Al	Si	S	Ca	Cl
Bottom ash											
Spot 1	-	4.53	19.5	73.9	0.84	-	-	-	-	1.2	-
Spot 2	0.36	15.6	50.4	15.8	15.2	0.31	0.21	-	-	1.9	0.3
Spot 3	0.6	11.9	18.3	67.6	0.9	-	-	-	-	-	0.64
Spot 4	-	5.05	15.7	78	0.8	-	-	-	-	-	-
Spot 5	-	4.3	28.3	67.4	-	-	-	-	-	-	-
Spot 6	0.8	2.4	27.4	51	-	2.7	-	-	-	15.8	-
Spot 7	1.8	24.7	39.8	17.6	0.4	2.4	0.4	0.6	-	12.5	-
Spot 8	0.6	10.6	22.3	58.9	-	1	-	-	-	6.61	-
Spot 9	-	11.6	-	88.4	-	-	-	-	-	-	-
Spot 10	9.5	3.9	34.3	10.2	-	5.4	0.6	0.9	-	35.2	-
Fly ash											
Spot I	0.74	23.54	16.60	30.18	1.86	0.97	3.44	-	1.28	3.04	18.36
Spot II	0.49	8.98	17.86	61.23	1.58	-	-	-	2.67	2.39	4.79
Spot III	0.50	18.28	41.71	16.20	11.87	-	0.33	-	1.03	6.09	4.01
Spot IV	0.76	10.67	44.29	12.56	2.65	-	-	17.84	0.51	10.09	0.64
Spot V	7.59	6.39	34.49	21.68	1.30	2.11	1.65	5.22	0.78	16.51	2.28
Spot VI	0.49	36.80	23.02	4.18	0.46	-	10.61	14.28	1.22	-	4.35
Spot VII	0.78	36.21	13.54	19.63	1.00	0.54	-	1.02	3.12	5.55	18.61
Spot VIII	-	4.82	19.98	20.41	0.67	1.61	-	24.78	0.69	25.30	1.66
Spot IX	-	3.19	15.73	78.64	-	-	-	-	0.66	1.10	0.68
Spot X	-	7.32	14.47	76.36	-	-	-	-	-	1.86	-
Spot XI	-	6.66	19.18	71.91	-	-	-	-	-	-	-
Window (a)	*	0.5	10.6	29.4	52.4	5.7	0.3	0.2	-	1.5	0.5
	**	0.2	5.6	18.2	31.9	8.2	0	0	-	0.5	0.2
	A.I	0.17 (Kg alkaline/GJ)									
Window (b)	A.I	0.06 (Kg alkaline/GJ)									
Window (c)	*	3.2	9.6	30.4	48.9	0.4	2.9	0.5	0.7	17.1	-
	**	4.3	8.3	6.7	30	0	1.9	0.2	0.2	12.9	-
	A.I	0.05 (Kg alkaline/GJ)									

510 * Average, ** Deviation

511 4. Conclusion

512 The understanding of biomass combustion behaviours, performances and their environmental
513 impact is a crucial consideration in terms of sustainable energy development. For this
514 purpose, the most frequent biomass in southwestern Morocco, namely argan nut shell (ANS),
515 was studied. Many conclusions can be drawn based on the experimental results of this work.
516 ANS was burnt in the laboratory furnace without any ash agglomeration problem. On
517 increasing the air flow, the combustion temperature, the FBR and the MCE of raw ANS
518 increased until a critical value which corresponds to 108 m³.h⁻¹ in our study. At this air flow
519 rate, less CO concentration is obtained and the ash content is almost negligible. High air

520 excess reduces the reaction time and consequently the flame temperature and the combustion
521 efficiency since the carbon conversion was limited. With the decrease in ANS length, the
522 combustion duration was shorter, which results in a rise in the FBR. However, the shortest
523 ANS biomass length (broken particles: BP) induced high CO concentration and consequently
524 lower MCE under low and moderate air flows (72 and 108 m³.h⁻¹, respectively). A high
525 excess of air supply, especially for the BP improved the FBR (better than wood pellets), the
526 combustion temperature, the emission of CO and the MCE. In all the cases studied, the
527 average NO_x emission was less than 140 mg.Nm⁻³ at 10% O₂. The flame had an irregular
528 shape for the longest ANS biomass but was more stable when the biomass particle size
529 decreased (BP). These facts indicate that a change in fuel specification clearly affects the
530 combustion process. Such results prove that ANS biomass may be an alternative fuel for
531 present and future energy production. Nevertheless, further work is required to study the
532 effect of secondary air on pollutant emissions (especially CO) of BP of ANS to ensure their
533 suitability for combustion. This will not only give further information on the combustion
534 characteristics of this biomass but also validate the presented results in this study.

535 **Nomenclature**

536	ANS	Argan nut shell
537	RP	Raw particles
538	LP	Large particles
539	SP	Small particles
540	BP	Broken particles
541	WP	Wood pellet
542	M	Moisture content (wet %)
543	VM	Volatile matter (wet %)
544	FC	Fixed carbon (wet %)

545	BD	Bulk density (kg.m^{-3})
546	LHV	Low heating value (MJ.kg^{-1})
547	ED	Energetic density (GJ.m^{-3})
548	AFR	Air fuel ratio (kg air/kg fuel)
549	TC	Thermocouple
550	FBR	Fuel burn rate (kg.s^{-1})
551	MCE	Modified combustion efficiency (%)
552	BBV	Biomass bed velocity ($\text{mm}^2.\text{s}^{-1}$)
553	SEM	Scanning electron microscopy
554	EDS	Energy dispersive x-ray spectroscopy
555	AI	Alkaline index (kg.GJ^{-1})

556

557 **Acknowledgements**

558 This work has been supported by the ANR (Agence National de la Recherche), EranetMed
 559 II RenewValue project. The technical help of Radouane Leghrib from LETSMP Ibn Zohr
 560 University is gratefully acknowledged.

561

562 **References**

- 563 [1] T. Kousksou, A. Allouhi, M. Belattar, A. Jamil, T. El Rhafiki, A. Arid, Y. Zeraouli,
 564 Renewable energy potential and national policy directions for sustainable development
 565 in Morocco, *Renew. Sustain. Energy Rev.* 47 (2015) 46–57,
 566 <https://doi.org/10.1016/j.rser.2015.02.056>.
- 567 [2] M. Balat, G. Ayar, Biomass energy in the world, use of biomass and potential trends,
 568 *Energy Sources.* 27 (2005) 931–940. <https://doi.org/10.1080/00908310490449045>.

- 569 [3] J. Werther, M. Saenger, E.-U. Hartge, T. Ogada, Z. Siagi, Combustion of agricultural
570 residues, *Prog. Energy Combust. Sci.* 26 (2000) 1–27. <https://doi.org/10.1016/S0360->
571 1285(99)00005-2.
- 572 [4] F.Z. Zouhair, A. Benali, M.R. Kabbour, K. EL Kabous, E. haj El Maadoudi, M.
573 Bouksaim, A. Essamri, Typical characterization of argane pulp of various Moroccan
574 areas: A new biomass for the second-generation bioethanol production, *J. Saudi Soc.*
575 *Agric. Sci.* (2018). <https://doi.org/10.1016/j.jssas.2018.09.004>.
- 576 [5] Nussbaumer Thomas, *Combustion and Co-combustion of Biomass: Fundamentals,*
577 *Technologies, and Primary Measures for Emission Reduction, Energy and Fuels.* 17
578 (2003) 1510–1521. <https://doi.org/10.1021/ef030031q>.
- 579 [6] A.K. Asthana, *Biomass as fuel in small boilers*, 2009. www.apo-tokyo.org.
- 580 [7] S. Khlifi, M. Lajili, F. Tabet, T. Boushaki, B. Sarh, Investigation of the combustion
581 characteristics of briquettes prepared from olive mill solid waste blended with and
582 without a natural binder in a fixed bed reactor, *Biomass Convers. Biorefinery.* (2019).
583 <https://doi.org/10.1007/s13399-019-00449-7>.
- 584 [8] A. Khor, C. Ryu, Y. bin Yang, V.N. Sharifi, J. Swithenbank, Straw combustion in a
585 fixed bed combustor, *Fuel.* 86 (2007) 152–160.
586 <https://doi.org/10.1016/j.fuel.2006.07.006>.
- 587 [9] Z. Cepic, B. Nakomcic-Smaragdakis, B. Miljkovic, L.Z. Radovanović,
588 S. Djuric, Combustion characteristics of wheat straw in a fixed bed,
589 *Energy Sources, Part A Recover. Util. Environ. Eff.* 38 (2016) 1007–
590 1013. <https://doi.org/10.1080/15567036.2014.922646>.
- 591 [10] M.M. Roy, A. Dutta, K. Corscadden, An experimental study of combustion and
592 emissions of biomass pellets in a prototype pellet furnace, *Appl. Energy.* 108 (2013)
593 298–307. <https://doi.org/10.1016/j.apenergy.2013.03.044>.

- 594 [11] Y. Elmay, G. Trouvé, M. Jeguirim, R. Said, Energy recovery of date palm residues in a
595 domestic pellet boiler, *Fuel Process. Technol.* 112 (2013) 12–18.
596 <https://doi.org/10.1016/j.fuproc.2013.02.015>.
- 597 [12] C. Ryu, Y. Bin Yang, A. Khor, N.E. Yates, V.N. Sharifi, J. Swithenbank, Effect of fuel
598 properties on biomass combustion: Part I. Experiments - Fuel type, equivalence ratio
599 and particle size, *Fuel.* 85 (2006) 1039–1046.
600 <https://doi.org/10.1016/j.fuel.2005.09.019>.
- 601 [13] Y. Rahib, T. Boushaki, B. Sarh, A. Ihlal, J. Chaoufi, S. Bonnamy, A. Elorf, Combustion
602 analysis of fixed beds of argan nut shell (ANS) biomass in batch type reactor, 2019 7th
603 International Renewable and Sustainable Energy Conference (IRSEC), Agadir,
604 Morocco, 2019, pp. 1-7, <https://doi.org/10.1109/IRSEC48032.2019.9078217>.
- 605 [14] T. Onabanjo, A.J. Kolios, K. Patchigolla, S.T. Wagland, B. Fidalgo, N. Jurado, D.P.
606 Hanak, V. Manovic, A. Parker, E. McAdam, L. Williams, S. Tyrrel, E. Cartmell, An
607 experimental investigation of the combustion performance of human faeces, *Fuel.* 184
608 (2016) 780–791. <https://doi.org/10.1016/j.fuel.2016.07.077>.
- 609 [15] X. Meng, R. Sun, T.M. Ismail, W. Zhou, X. Ren, R. Zhang, Parametric studies
610 on corn combustion characteristics in a fixed bed: Primary air flow rate and
611 different corn lengths, *Appl. Therm. Eng.* 126 (2017) 702–716.
612 <https://doi.org/10.1016/j.applthermaleng.2017.07.197>.
- 613 [16] Y. Rahib, B. Sarh, J. Chaoufi, S. Bonnamy, A. Elorf, Physicochemical and thermal
614 analysis of argan fruit residues (AFRs) as a new local biomass for bioenergy production,
615 *J. Therm. Anal. Calorim.* (2020). <https://doi.org/10.1007/s10973-020-09804-7>.
- 616 [17] TSI, [Combustion Analysis Basics: An Overview of Measurements, Methods and](#)
617 [Calculations Used in Combustion Analysis, 2004.](#)

- 618 [18] R. García, C. Pizarro, A.G. Lavín, J.L. Bueno, Biomass sources for thermal
619 conversion. Techno-economical overview, *Fuel*. 195 (2017) 182–189.
620 <https://doi.org/10.1016/j.fuel.2017.01.063>.
- 621 [19] Y. Rahib, A. Elorf, B. Sarh, S. Bonnamy, J. Chaoufi, M. Ezahri, Experimental analysis
622 on thermal characteristics of argan nut shell (ANS) biomass as a green energy resource,
623 *Int. J. Renew. Energy Res.* 9 (2019) 1606–16015.
- 624 [20] Y. Rahib, B. Sarh, S. Bostyn, S. Bonnamy, T. Boushaki, J. Chaoufi, Non-isothermal
625 kinetic analysis of the combustion of argan shell biomass, *Mater. Today Proc.* (2020)
626 11–16. <https://doi.org/10.1016/j.matpr.2019.07.437>.
- 627 [21] G. Leyssens, G. Trouvé, I. Caplain, C. Schönnenbeck, F. Cazier, Energetic
628 performances and environmental impact of the combustion of cardboard/sawdust in a
629 domestic boiler, *Fuel*. 122 (2014) 21–27. <https://doi.org/10.1016/j.fuel.2014.01.034>.
- 630 [22] S. Polesek-Karczewska, T. Turzyński, D. Kardaś, Heda, Front velocity in the
631 combustion of blends of poultry litter with straw, *Fuel Process. Technol.* 176 (2018)
632 307–315. <https://doi.org/10.1016/j.fuproc.2018.03.040>.
- 633 [23] Y. Yuzuriha, W. Gao, T. Mogi, R. Dobashi, Effects of particle size distributions on
634 flame propagation behavior through dust clouds of PMMA, *J. Loss Prev. Process Ind.*
635 49 (2017) 852–858. <https://doi.org/10.1016/j.jlp.2017.06.011>.
- 636 [24] S.A. El-Sayed, M. Khairy, An experimental study of combustion and emissions of
637 wheat straw pellets in high-temperature air flows, *Combust. Sci. Technol.* 190 (2018)
638 222–251. <https://doi.org/10.1080/00102202.2017.1381953>.
- 639 [25] A.I. Calvo, L.A.C. Tarelho, C.A. Alves, M. Duarte, T. Nunes, Characterization of
640 operating conditions of two residential wood combustion appliances, *Fuel Process.*
641 *Technol.* 126 (2014) 222–232. <https://doi.org/10.1016/j.fuproc.2014.05.001>.

- 642 [26] G. Wielgosinski, P. Lechtanska, O. Namiecińska, Emission of some pollutants from
643 biomass combustion in comparison to hard coal combustion, *J. Energy Inst.* 90 (2017)
644 787–796. <https://doi.org/10.1016/j.joei.2016.06.005>.
- 645 [27] S. Luo, B. Xiao, Z. Hu, S. Liu, M. He, Experimental study on combustion of biomass
646 micron fuel (BMF) in cyclone furnace, *Energy Convers. Manag.* 51 (2010) 2098–2102.
647 <https://doi.org/10.1016/j.enconman.2010.03.001>.
- 648 [28] H. Khodaei, F. Guzzomi, D. Patiño, B. Rashidian, G.H. Yeoh, Air staging strategies in
649 biomass combustion-gaseous and particulate emission reduction potentials, *Fuel*
650 *Process. Technol.* 157 (2017) 29–41. <https://doi.org/10.1016/j.fuproc.2016.11.007>.
- 651 [29] U. Kleinhans, C. Wieland, F.J. Frandsen, H. Spliethoff, Ash formation and deposition in
652 coal and biomass fired combustion systems: Progress and challenges in the field of ash
653 particle sticking and rebound behavior, *Prog. Energy Combust. Sci.* 68 (2018) 65–168,
654 <https://doi.org/10.1016/j.pecs.2018.02.001>.
- 655 [30] T. Blomberg, Free alkali-index for optimizing the fuel mixture in biomass co-firing,
656 *Heat Exch. Fouling Clean.* VII. (2007) 14.
- 657 [31] M. Brostrom, S. Enestam, R. Backman, K. Mäkelä, Condensation in the KCl-NaCl
658 system, *Fuel Process. Technol.* 105 (2013) 142–148.
659 <https://doi.org/10.1016/j.fuproc.2011.08.006>.
- 660